FULL LENGTH	Iranian Biomedical Journal 30 (4): 225-233 July 2026

Tropolone Derivative JO-122(2) Enhances Temozolomide Efficacy and p53-Mediated Apoptosis in Glioblastoma Xenografts

Oleg I. Kit[1], Aleksey Yu. Maksimov[1], Igor V. Golovinov[1*], Natalia S. Kuznetsova[1], Irina V. Kaplieva[1], Daria V. Khodakova[1], Alexander B. Sagakyants[1], Anastasia V. Galina[1], Anna A. Shulga[1], Sofya V. Gurova[1], Elena S. Bondarenko[1], Eduard E. Rostorguev[1], Yurii A. Sayapin[2], Eugeny A. Gusakov[3]

[1]Federal State Budgetary Institution "National Medical Research Centre for Oncology" of the Ministry of Health of the Russian Federation, Rostov-on-Don, Russian Federation; [2]Federal State Budgetary Institution of Science "Federal Research Centre Southern Scientific Centre of the Russian Academy of Sciences" (SSC RAS), Rostov-on-Don, Russian Federation; [3]Research Institute of Physics and Chemistry, Southern Federal University, Rostov-on-Don, Russian Federation

OPEN ACCESS

Article type: Research Article
Received: February 21, 2026
Revised: June 1, 2026
Accepted: June 22, 2026
Published online: June 24, 2026

How to cite:
Kit OI, Maksimov AY, Golovinov IV, Kuznetsova NS, Kaplieva IV, Khodakova DV, Sagakyants AB, Galina AV, Shulga AA, Gurova SV, Bondarenko ES, Rostorguev EE, Sayapin YA, Gusakov EA. Tropolone Derivative JO-122(2) Enhances Temozolomide Efficacy and p53-Mediated Apoptosis in Glioblastoma Xenografts. *Iran. Biomed. J.* 2026; 30 (4): 225-233.

This article is licensed under a Creative Commons Attribution-NonDerivatives 4.0 International License.

ABSTRACT

Background: Glioblastoma (GBM) is the most aggressive primary brain tumor in adults, with limited therapeutic options and poor survival. Resistance to standard temozolomide (TMZ) therapy remains a major challenge, necessitating novel agents. Tropolone derivatives, particularly the synthetic trichlorotropolone JO-122(2), have shown broad preclinical antitumor activity. This study aimed to determine whether JO-122(2), alone or combined with TMZ, can suppress GBM growth in vivo and to define the accompanying changes in the p53/MDM2/Bcl-2 apoptotic axis.

Methods: JO-122(2), as monotherapy or combined with TMZ, was evaluated in a U87 MG GBM xenograft model in BALB/c nude mice (n = 8 per group). Tumor volumes were monitored over 25 days, and tumor growth inhibition (TGI) was calculated. Molecular mechanisms were investigated by RT-qPCR and ELISA, assessing gene expression and protein levels of the apoptotic regulators *TP53*, *MDM2*, *BAX*, *BCL2*, and *CASP9*.

Results: JO-122(2) and TMZ monotherapy inhibited tumor growth (TGI = 42.08% and 61.44%, respectively). The combination therapy reduced tumor volume 4.9-fold compared to the vehicle control and achieved a TGI of 79.88% ($p = 4.20 \times 10^{-8}$ vs. control; $p = 1.66 \times 10^{-3}$ vs. TMZ; $p = 5.97 \times 10^{-5}$ vs. JO-122(2)). It also increased p53, Bax, and caspase-9 protein levels and decreased MDM2 and Bcl-2, with concordant upregulation of *TP53* and *BAX* and downregulation of *MDM2* and *BCL2* mRNA, indicating modulation of the p53/MDM2/Bcl-2 axis.

Conclusion: JO-122(2) exerts potent antitumor effects in GBM, particularly when combined with TMZ, by promoting mitochondrial apoptosis through the coordinated regulation of p53 and its downstream effectors.
DOI: 10.22034/IBJ.30.4.225

Keywords: Apoptosis, Glioblastoma, p53, Temozolomide, Tropolone

Corresponding Author: Golovinov Igor V.
Federal State Budgetary Institution "National Medical Research Centre for Oncology" of the Ministry of Health of the Russian Federation, Rostov-on-Don, Russian Federation; Tel.: (+7-928) 1318752; E-mail: ivgolovinov@yandex.ru; ORCID ID: 0000-0003-3011-6904

[Downloaded from ibj1.pasteur.ac.ir on 2026-10-16]

[DOI: 10.22034/IBJ.30.4.225]

1. INTRODUCTION

Glioblastoma (GBM), a WHO grade IV glioma, is the most prevalent and aggressive primary brain tumor in adults[1], accounting for about 30% of all central nervous system (CNS) tumors and 80% of primary malignant CNS neoplasms[2]. Despite standard multimodal therapies (surgery, radiotherapy, and temozolomide [TMZ]), GBM prognosis remains poor, with a median survival of 15–18 months[2,3]. While radiotherapy and TMZ synergistically induce DNA damage in tumors[2]. GBM frequently develops intrinsic and acquired resistance via enhanced DNA repair and drug tolerance, compromising efficacy. This condition underscores the urgent need for novel and selective therapeutics.

Nitrogen-containing bicyclic heterocycles have emerged as promising chemotherapeutic agents[4]. Tropolone derivatives, in particular, exhibit broad biological activities, including potent antitumor effects[5-7]. Their polypharmacological profile, mediated by kinase inhibition, tubulin disruption, and apoptosis induction[8], makes them potential candidates for novel anticancer therapies[9,10].

The synthetic tropolone derivative JO-122(2) (2-(1,1-dimethyl-1H-benzo[e]indolin-2-yl)-5,6,7-trichloro-1,3-tropolone) has demonstrated potent preclinical antitumor activity in the models of gastric adenocarcinoma patient-derived xenografts and U87 MG GBM xenograft[11,12]. Other related compounds have shown diverse mechanisms of action; hinokitiol inhibits lung cancer cell migration via the NF-κB/MMPs pathway[13], copper-tropolone complexes surpass cisplatin in breast cancer[5], and quinoline-substituted trichlorotropolone derivatives show efficacy in non-small cell lung cancer[14]. Collectively, these data highlight the potential of this class of compounds for targeting oncogenic processes. To address this therapeutic need, we evaluated JO-122(2) alone and in combination with TMZ in a U87 MG xenograft model, focusing on its molecular effects on key apoptotic regulators: p53, MDM2, Bcl-2/Bax ratio, and caspase-9.

2. MATERIALS AND METHODS

2.1. Chemicals and reagents

The tropolone derivative JO-122(2) was synthesized at the Research Institute of Physical and Organic Chemistry, Southern Federal University (Rostov-on-Don, Russia). TMZ was purchased from BIOCAD (Saint Petersburg, Russia). Cell culture reagents (RPMI-1640, DMEM, FBS, L-glutamine, and antibiotics) were sourced from Gibco, Himedia, PanEco, and Biolot. The structural identity and chemical purity (≥98%) of JO-122(2) were confirmed by comprehensive spectroscopic analysis ($^{1}H/^{13}C$ NMR, IR, MS) and elemental analysis prior to biological testing. Full spectral datasets and detailed synthetic protocols are documented in Russian Federation Patents RU 2810581 C1 and RU 2839886 C1[15,16]. Due to limited aqueous solubility, a standardized oral formulation was prepared by dissolving JO-122(2) in DMSO and diluting with 1% starch suspension to achieve a final DMSO concentration of 10% (v/v). This concentration falls within the established safety thresholds for murine oral gavage and caused no local irritation or systemic toxicity in pilot studies. Suspensions were prepared extemporaneously, visually inspected for homogeneity, and administered within 30 min to ensure the stability of the trichlorotropolone scaffold under physiological conditions[17,18]. Dosing was performed using flexible 20–22 G oral gavage needles, with volumes strictly maintained ≤10 mL/kg.

2.2. Cell culture

Human GBM U87 MG cells were obtained from the National Medical Research Centre for Oncology (Rostov-on-Don). Authentication of these cells was confirmed by STR profiling (COrDIS Plus kit, Gordiz), and routine mycoplasma testing was performed by PCR (Servicebio, China). All experiments utilized mycoplasma-negative cultures at passages 35–39. Cells were maintained in DMEM or RPMI-1640 supplemented with 10% FBS, 2 mM L-glutamine, 100 U/mL penicillin, and 100 µg/mL streptomycin. The dual-medium approach reflected reagent availability during the study; both formulations supported equivalent proliferation kinetics. Cultures were incubated in 5% CO_2 with 95% humidity at 37°C and passaged at 80% confluency using standard trypsin-EDTA protocols.

2.3. In vivo xenograft model

Immunodeficient BALB/c nude mice (5–6 weeks old) were housed in a specific-pathogen-free vivarium using individually ventilated cages (Tecniplast, Italy). Environmental parameters were strictly controlled (temperature 21–26°C, relative humidity 50–60%, a 12-h light/dark cycle), with autoclaved food/water provided ad libitum. For xenograft establishment, U87 MG cells at 75–85% confluency were trypsinized, washed with PBS, and resuspended in serum-free RPMI-1640 at 25 × 10^6 viable cells/mL to prevent xenogeneic protein introduction. A 0.2 mL aliquot (5 × 10^6 cells) was injected subcutaneously into the right flank. Animals were randomized into experimental cohorts using a computer-generated sequence and stratified to ensure comparable baseline tumor volumes (100 ± 20 mm^3). Tumor measurements were performed blindly by trained personnel using digital calipers. Predefined humane endpoints included tumor volume >2,000 mm^3, ulceration/necrosis, >20% body weight loss, or severe

[Downloaded from ibj1.pasteur.ac.ir on 2026-10-16]

[DOI: 10.22034/IBJ.30.4.225]

clinical distress. All animals were monitored daily by veterinary staff; no subject reached termination criteria.

2.4. Treatment protocol, efficacy assessment, and safety monitoring

Mice were allocated into four groups (n = 8/group) and treated for 25 days. Group 1 received TMZ (20 mg/kg, i.p., daily); group 2 received JO-122(2) (60 mg/kg, by oral gavage, three times weekly); group 3 received the combination at the same doses and schedules; group 4 received a vehicle control (0.9% NaCl, i.p., daily + 1% starch/10% DMSO, by oral gavage, three times weekly, ≤300 μL). Dose selection followed a stepwise preclinical validation strategy. Initial in vitro profiling in U87 MG cells demonstrated G_0/G_1 cell cycle arrest and caspase-dependent apoptosis (IC_{50} = 1.96 μM at 72 h)[19]. Subsequent in vivo dose-ranging studies (10–60 mg/kg) established 60 mg/kg as the optimal therapeutic dose, achieving maximal tumor growth inhibition (TGI) of 39.54% without systemic toxicity[20]. This dose aligns with efficacy data for structurally related trichlorotropolone derivatives (~55 mg/kg) in NSCLC xenograft models[14]. The TMZ regimen (20 mg/kg, i.p., daily) was selected to replicate clinical pharmacokinetic profiles and ensure reproducible antitumor activity in U87 MG models[21]. All administrations were performed between 09:00 and 11:00 AM to minimize circadian pharmacokinetic variability. Tumor dimensions were measured every three days. Volume (mm³) was calculated as $V = (L \times W^2)/2$, where L is the longest diameter and W is the perpendicular width. Antitumor efficacy was evaluated using two complementary metrics. Terminal TGI at day 25 was calculated as $TGI (\%) = ((V_c - V_t)/V_c) \times 100$, where V_c and V_t represent mean tumor volumes in control and treated groups, respectively. Longitudinal tumor burden was assessed using the area under the volume-time curve (AUC_{1-25}), computed using the trapezoidal rule: $AUC = \sum_{i=1}^{n-1} \frac{(V_i+V_{i+1})}{2} \times (t_{i+1} - t_i)$; Relative AUC reduction was determined as $\text{AUC reduction } (\%) = \left(1 - \frac{AUC_{treated}}{AUC_{control}}\right) \times 100$. Systemic toxicity was monitored through daily clinical assessments and body weight measurements (baseline, then every 72 h). No treatment-related weight loss (>10%) or behavioral abnormalities were observed. These safety findings corroborate prior dose-ranging research, confirming the absence of mortality, hematological/biochemical deviations, or organ toxicity[20]. Notably, JO-122(2) attenuated tumor-induced systemic complications, including anemia, leukopenia, and hyperglycemia. All procedures adhered to strict humane endpoint enforcement and daily veterinary oversight.

2.5. Gene expression analysis (RT-qPCR)

Total RNA was extracted from excised tumor tissues using TRIzol reagent (Thermo Fisher Scientific, USA). Complementary DNA synthesis was performed using a commercial reverse transcription kit (Syntol, Russia). For qPCR, SYBR Green master mix (Syntol) was used on a DTprime real-time PCR system (DNA-Technology, Russia). The primer sequences are provided in Table 1. Gene expression was normalized to the *ACTB* gene, which demonstrated stable amplification across all groups (mean Ct = 18.6 ± 0.9; CV <5%). Relative quantification was performed using the $2^{-\Delta\Delta Ct}$ method. All RT-qPCR assays were conducted in three biological and technical replicates to ensure statistical robustness.

2.6. Protein analysis (ELISA)

Tumor tissues were homogenized using a BD Medimachine system (BD Biosciences, USA) and centrifuged (3,000 ×g, 4°C, 10 min). Supernatants were analyzed for p53, MDM2, Bax, Bcl-2, and caspase-9 using commercial sandwich ELISA kits (Cloud-Clone Corp., USA; cat. nos. SEA928Hu, SEG790Hu, SEB343Hu, SEA778Hu, SEA627Hu) as per manufacturer's protocols. The minimum detectable concentrations for the proteins were as follows: p53 (27 pg/mL), MDM2 (0.055 ng/mL), Bax (28.2 pg/mL), Bcl-2 (0.056 ng/mL), caspase-9 (0.121 ng/mL). Absorbance was measured at 450 nm (reference wavelength of 630 nm) on an MR-96A microplate reader (Mindray, China). Washing/incubation steps were automated (StatFax-2600/2200, Awareness Technology, USA). Protein levels were normalized to tissue weight (pg/mg or ng/mg). Standard curves were generated via serial dilutions of recombinant standards and interpolated

Table 1. Primer sequences used in RT-qPCR

Gene	Forward primer sequence	Reverse primer sequence
TP53	ACCCTCTGACCTTTTTCCCA	TGCTGGGATCTTAGGCACTC
MDM2	ACCCTGGTTAGACCAAAGCC	TGGCACGCCAAACAAATCTC
BAX	TGGCAGCTGACATGTTTTCTGAC	TCACCCAACCACCCTGGTCTT
BCL2	TCGCCCTGTGGATGACTGA	CAGAGACAGCCAGGAGAAATCA
CASP9	CTCTACTTTCCCAGGTTT	TTTCACCGAAACAGCATT

[Downloaded from ibj1.pasteur.ac.ir on 2026-10-16]

[DOI: 10.22034/IBJ.30.4.225]

using four-parameter logistic (4-PL) regression. As these kits quantify total protein without distinguishing post-translationally modified or cleaved isoforms (e.g., active caspase-9), data interpretation was integrated with RT-qPCR profiles, functional endpoints, and established mechanistic literature. All assays were performed in three independent biological replicates.

2.7. Statistical analysis

Analyses were conducted in Statistica 10 (StatSoft, USA) and Excel 2013. Normality was assessed using the Shapiro-Wilk test. Pairwise comparisons among groups were performed using Welch's unequal-variance t-test, and the resulting *p* values were adjusted for the six pairwise comparisons among the four experimental groups using the Bonferroni method. All *p* values reported in the text, figures, and tables are Bonferroni-adjusted; significance was set at adjusted $p < 0.05$. Data are presented as mean ± standard deviation (SD). Each cohort included four male and four female mice; two-way ANOVA (sex × treatment) revealed no significant sex effects or interactions for primary endpoints (all $p > 0.05$), permitting data pooling. Concordance between transcriptional and translational regulation was evaluated using Pearson correlation (R) between $\log_2$-fold mRNA changes (RT-qPCR) and protein concentrations (ELISA) for *TP53*, *MDM2*, *BAX*, *BCL2*, and *CASP9*. Correlation strength was interpreted as: |R| ≥0.8 (strong), 0.5≤ |R| <0.8 (moderate), |R| <0.5 (weak).

3. RESULTS

3.1. Antitumor efficacy of JO-122(2) and TMZ in vivo

Antitumor activity of JO-122(2) was evaluated in U87 MG xenografts (n = 8/group, balanced sex). No sex-related differences were detected; hence, the data were pooled. Tumor growth suppression emerged on day 11 for TMZ and combination groups, and day 13 for JO-122(2) monotherapy. At the endpoint (day 25), the size of control tumors was 1387.44 ± 141.45 mm³. TMZ monotherapy reduced tumor volume by 2.6-fold (535.02 ± 98.50 mm³), JO-122(2) monotherapy resulted in a 1.7-fold reduction (803.59 ± 146.07 mm³), and the combination yielded a 4.9-fold reduction (279.14 ± 58.94 mm³; $p = 4.20 \times 10^{-8}$ vs. control). The combination treatment was more effective than monotherapies (TMZ: $p = 1.66 \times 10^{-3}$; JO-122(2): $p = 5.97 \times 10^{-5}$; Fig. 1). TGI reached 79.88% for the combination therapy, 61.44% for TMZ, and 42.08% for JO-122(2). Longitudinal AUC_{1-25} analysis confirmed these findings as follows: control 16,529.09 mm³·days; TMZ 8,533.96 mm³·days (48.37% reduction); JO-122(2) 11,508.80 mm³·days (30.37% reduction); combination therapy 7,740.20 mm³·days (53.17% reduction).

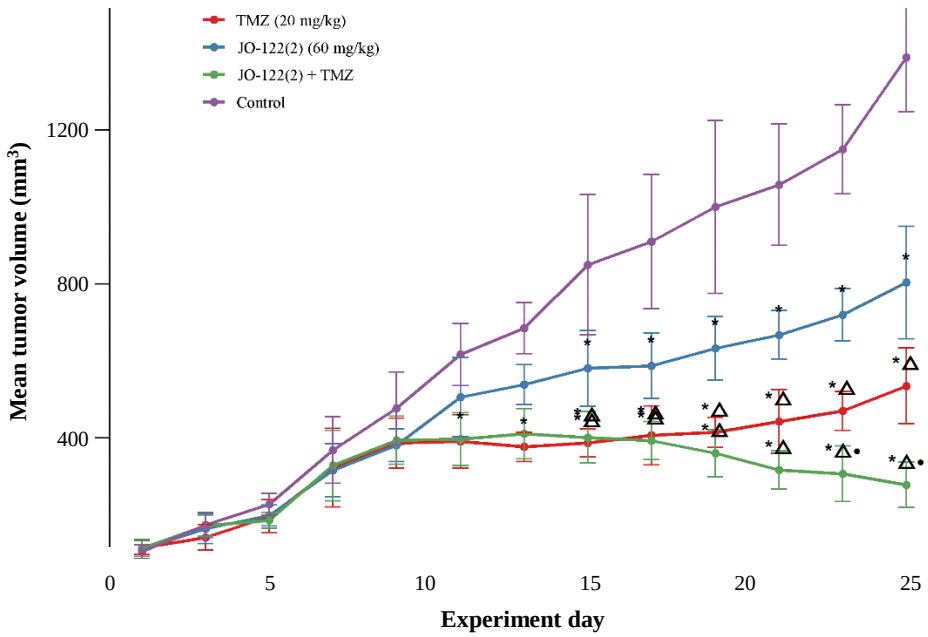

Fig. 1. Tumor growth kinetics in U87 MG xenografts following treatment with TMZ (20 mg/kg, intraperitoneally, daily), JO-122(2) (60 mg/kg, by oral gavage, three times weekly), and the combination, or a vehicle control over 25 days. Tumor volume (mm³) was calculated as $V = (L \times W^2)/2$ and measured every three days starting from the first day of treatment. Data are presented as the mean ± SD for n = 8 mice per group (four males and four females). Statistical significance was assessed as described in Section 2.7; adjusted *p* values are reported: *adjusted $p < 0.05$ vs. vehicle control group; •adjusted $p < 0.05$ vs. TMZ monotherapy group; △adjusted $p < 0.05$ vs. JO-122(2) monotherapy group.

[Downloaded from ibj1.pasteur.ac.ir on 2026-10-16]

[DOI: 10.22034/IBJ.30.4.225]

3.2. Results for gene expression and protein level determinations

Protein and mRNA levels of apoptotic regulators are summarized in Tables 2 and 3. The combination group showed the highest p53 protein concentration (5091.64 ± 590.22 pg/mg), exceeding the control (2650.45 ± 923.65 pg/mg; 1.9-fold, $p = 2.46 \times 10^{-4}$) and TMZ monotherapy (3506.84 ± 369.77 pg/mg; $p = 2.13 \times 10^{-4}$) groups. JO-122(2) monotherapy also elevated p53 protein expression (4428.49 ± 410.93 pg/mg) compared to the control ($p = 3.70 \times 10^{-3}$) and TMZ ($p = 2.05 \times 10^{-3}$). *TP53* mRNA was significantly elevated in JO-122(2) monotherapy ($\log_2$FC: 0.42 ± 0.23; $p = 8.61 \times 10^{-4}$) and combination therapy ($\log_2$FC: 0.49 ± 0.28; $p = 1.28 \times 10^{-3}$) compared to the control. TMZ monotherapy also produced a smaller but statistically significant increase in *TP53* mRNA relative to the control ($\log_2$FC: 0.26 ± 0.23; $p = 3.87 \times 10^{-2}$). MDM2 protein levels were most strongly suppressed by combination therapy (0.27 ± 0.10 ng/mg; ~4-fold vs. control 1.08 ± 0.27 ng/mg; $p = 1.49 \times 10^{-4}$), and also JO-122(2) (0.32 ± 0.08 ng/mg; $p = 3.17 \times 10^{-4}$) and TMZ (0.54 ± 0.04 ng/mg; p = 4.23 × 10^{-3}) monotherapy compared to control. Both JO-122(2) and combination therapy also significantly suppressed MDM2 compared to TMZ alone ($p = 2.03 \times 10^{-4}$ and $p = 3.10 \times 10^{-4}$, respectively). *MDM2* mRNA showed a significant downregulation compared to control in all treatment groups: TMZ ($\log_2$FC: -0.62 ± 0.23; $p = 3.60 \times 10^{-4}$), JO-122(2) ($\log_2$FC: -1.25 ± 0.30; $p = 6.94 \times 10^{-6}$), and combination therapy ($\log_2$FC: -1.51 ± 0.36; $p = 7.73 \times 10^{-6}$). The combination therapy downregulated *MDM2* mRNA more strongly than TMZ alone ($p = 2.83 \times 10^{-3}$), and JO-122(2) monotherapy downregulated it more strongly than TMZ monotherapy ($\log_2$FC −1.25 ± 0.30 vs. −0.62 ± 0.23; p = 1.25 × 10^{-2}). Bax protein levels peaked in the combination group (3967.93 ± 751.33 pg/mg), significantly exceeding those of TMZ (2979.73 ± 382.30 pg/mg; $p = 4.45 \times 10^{-2}$). JO-122(2) monotherapy also elevated Bax levels (3781.16 ± 760.40 pg/mg). *BAX* mRNA was significantly upregulated compared to control in JO-122(2) monotherapy ($\log_2$FC: 0.77 ± 0.25; $p = 1.26 \times 10^{-4}$) and combination therapy ($\log_2$FC: 0.89 ± 0.25; p = 3.53 × 10^{-5}), but not in TMZ monotherapy ($\log_2$FC: 0.14 ± 0.30). The combination therapy also upregulated *BAX* mRNA relative to TMZ ($p = 4.84 \times 10^{-3}$), and JO-122(2) monotherapy upregulated *BAX* mRNA more strongly than TMZ monotherapy ($\log_2$FC 0.77 ± 0.25 vs. 0.14 ± 0.30; $p = 1.58 \times 10^{-2}$). The elevated SD for Bax in the control group reflects inherent biological heterogeneity in untreated xenograft tissues; however, all intergroup comparisons remained statistically robust following Bonferroni correction and were further validated by strong transcriptional-translational concordance (R = 0.90). Bcl-2 protein concentration was the lowest in the combination group (0.21 ± 0.08 ng/mg) and significantly reduced compared to control (1.54 ± 0.67 ng/mg; $p = 4.56 \times 10^{-3}$), TMZ (1.04 ± 0.29 ng/mg; $p = 3.01 \times 10^{-4}$), and JO-122(2) (0.42 ± 0.14 ng/mg; $p = 2.12 \times 10^{-2}$). JO-122(2) monotherapy also significantly reduced Bcl-2 compared to control ($p = 1.16 \times 10^{-2}$) and TMZ ($p = 1.64 \times 10^{-3}$). *BCL2* mRNA was strongly downregulated compared to control by combination therapy ($\log_2$FC: -1.74 ± 0.42; $p = 7.68 \times 10^{-6}$) and JO-122(2) monotherapy ($\log_2$FC: -1.34 ± 0.35; $p = 1.74 \times 10^{-5}$), but not by TMZ monotherapy ($\log_2$FC: -0.15 ± 0.28). Combination therapy also significantly downregulated *BCL2* mRNA compared to TMZ alone ($p = 9.62 \times 10^{-5}$), and JO-122(2) monotherapy downregulated *BCL2* mRNA more strongly than TMZ monotherapy ($\log_2$FC -1.34 ± 0.35 vs. -0.15 ± 0.28; $p = 4.39 \times 10^{-4}$). Caspase-9 protein levels were significantly elevated in JO-122(2)-containing groups compared to control: JO-122(2) monotherapy (2.74 ± 0.54 ng/mg vs. control 1.18 ± 0.59 ng/mg; $p = 4.65 \times 10^{-4}$) and also combination therapy (3.10 ± 0.77 ng/mg vs. control; $p = 5.24 \times 10^{-4}$). Both JO-122(2) and combination therapy also significantly elevated caspase-9 compared to TMZ monotherapy (1.24 ± 0.48 ng/mg; $p = 2.54 \times 10^{-4}$ and $p = 5.91 \times 10^{-4}$, respectively). *CASP9* mRNA showed a non-significant upward trend with combination therapy ($\log_2$FC: 0.27 ± 0.23). Pearson correlations between the $\log_2$-fold change of each transcript and the concentration of its protein

Table 2. Protein levels in tumor tissue normalized to tissue mass following treatment with TMZ, JO-122(2), their combination, or vehicle control

Protein	TMZ (20 mg/kg)	JO-122(2) (60 mg/kg)	JO-122(2) (60 mg/kg) + TMZ (20 mg/kg)	Control
p53 (pg/mg)	3506.84 ± 369.77	4428.49 ± 410.93*•	5091.64 ± 590.22*•	2650.45 ± 923.65
MDM2 (ng/mg)	0.54 ± 0.04*	0.32 ± 0.08*•	0.27 ± 0.10*•	1.08 ± 0.27
Bax (pg/mg)	2979.73 ± 382.30	3781.16 ± 760.40	3967.93 ± 751.33·	3151.16 ± 1190.14
Bcl-2 (ng/mg)	1.04 ± 0.29	0.42 ± 0.14*•	0.21 ± 0.08*•△	1.54 ± 0.67
Caspase-9 (ng/mg)	1.24 ± 0.48	2.74 ± 0.54*•	3.10 ± 0.77*•	1.18 ± 0.59

Data are expressed as mean ± SD (n = 8 per group). *adjusted $p < 0.05$ vs. control group; •adjusted $p < 0.05$ vs. TMZ monotherapy; △adjusted $p < 0.05$ vs. JO-122(2) monotherapy. Bonferroni-adjusted p values from pairwise comparisons, as described in Section 2.7.

[Downloaded from ibj1.pasteur.ac.ir on 2026-10-16]

[DOI: 10.22034/IBJ.30.4.225]

Table 3. Gene expression in tumor tissues

Treatment regimen	*TP53*	*MDM2*	*BAX*	*BCL2*	*CASP9*
TMZ (20 mg/kg)	0.26 ± 0.23*	-0.62 ± 0.23*	0.14 ± 0.30	-0.15 ± 0.28	-0.07 ± 0.22
JO-122(2) (60 mg/kg)	0.42 ± 0.23*	-1.25 ± 0.30*•	0.77 ± 0.25*•	-1.34 ± 0.35*•	0.07 ± 0.23
JO-122(2) (60 mg/kg) + TMZ (20 mg/kg)	0.49 ± 0.28*	-1.51 ± 0.36*•	0.89 ± 0.25*•	-1.74 ± 0.42*•	0.27 ± 0.23

Data presented as $\log_2$ fold change ± SD relative to vehicle control following treatment with TMZ, JO-122(2), or their combination *adjusted $p < 0.05$ vs. control group; •adjusted $p < 0.05$ vs. TMZ monotherapy. Bonferroni-adjusted p-values from pairwise comparisons, as described in Section 2.7.

product were strong: *TP53*/p53 (R = 0.98), *MDM2*/MDM2 (R = 0.96), *BAX*/Bax (R = 0.90), *BCL2*/Bcl-2 (R = 0.96), and *CASP9*/caspase-9 (R = 0.87). Bax and Bcl-2 protein levels showed a strong inverse correlation (R = -0.88), confirming coordinated transcriptional-translational regulation of the p53/MDM2/Bcl-2 apoptotic axis.

4. DISCUSSION

Mechanistically, combination therapy using JO-122(2) and TMZ modulates the p53/MDM2 axis, shifting cellular equilibrium toward intrinsic apoptosis. The pronounced downregulation of MDM2 at both the transcript and the protein level disrupts the negative feedback of MDM2 on p53 and thereby allows p53 to accumulate. Concurrently, the transcriptional suppression of *BCL2*, coupled with *BAX* induction, alters the Bcl-2/Bax ratio, a critical determinant of mitochondrial outer membrane permeabilization. These upstream shifts culminate in the elevated caspase-9 abundance, providing a molecular framework for the enhanced antitumor efficacy observed in treated xenografts.

The broad cytotoxic potential of tropolone derivatives across multiple malignancies—including AGS gastric adenocarcinoma, primary glioma, and SW620 colorectal cells[22-24], as well as ovarian, colon, lung, and pancreatic carcinoma lines[25]—highlights their capacity to target fundamental oncogenic pathways. In our U87 MG GBM xenograft model, the synthetic derivative JO-122(2) demonstrated significant antitumor activity, which was markedly enhanced when combined with TMZ. The observed MDM2 suppression may involve the hydroxyketone moiety of the tropolone scaffold, which theoretically confers metal-chelating properties that could disrupt zinc-dependent domains such as the MDM2 RING finger. However, direct binding or enzymatic inhibition was not experimentally assessed. Instead, the pronounced transcriptional downregulation of *MDM2*, coupled with p53 accumulation, suggests that JO-122(2) acts primarily through upstream regulatory networks or microRNA-mediated mechanisms, as previously described for structurally related tropolone derivatives[26-31]. This mechanism aligns with our findings indicating elevated p53 protein levels despite only moderate transcriptional upregulation of *TP53*, highlighting the dominance of post-translational regulation in the combination group[30-32].

The disruption of the p53-MDM2 negative feedback loop may be partially mediated by microRNAs, particularly miR-29a, which binds to the 3′-UTR of *MDM2* mRNA to suppress translation and facilitate degradation[26,29,31,32]. Downstream of p53 activation, the favorable shift in the Bcl-2/Bax ratio and the activation of caspase-9 indicate robust induction of mitochondrial apoptosis. Notably, caspase-9 activation occurred without significant upregulation of *CASP9* mRNA, which is consistent with its canonical post-translational activation within the apoptosome[30,33-36]. While increased total caspase-9 protein supports engagement of the intrinsic pathway, direct validation of proteolytic cleavage and executioner caspase activation remains a priority for future studies. Although NF-κB inhibition by related tropolones (e.g., hinokitiol) may further reinforce pro-apoptotic signaling[37,38], this pathway was not assessed herein. While other agents such as colchicine and quinoline-tropolone hybrids have been shown to downregulate Bcl-2[36,39,40], our data emphasize that JO-122(2) enhances intrinsic apoptosis primarily through the modulation of the p53/MDM2/Bcl-2 axis.

This study has several limitations. First, it assessed total p53 protein and transcriptional changes in p53-responsive genes without direct functional assays (e.g., phospho-specific immunodetection or DNA-binding assays); thus, while *BAX* upregulation and *MDM2*/*BCL2* downregulation are consistent with enhanced p53 pathway activity, indirect mechanisms cannot be definitively excluded. The subcutaneous U87 MG model does not fully recapitulate the orthotopic brain microenvironment or blood-brain barrier challenges; however, the molecular weight of JO-122(2) (418.70 g/mol) falls below the ~500 g/mol threshold for passive diffusion, providing a theoretical basis for CNS bioavailability. Comparative cytotoxicity profiling against non-malignant human cell lines was not performed, though comprehensive in vivo safety assessments at 60 mg/kg revealed no systemic toxicity. Tumor growth was rigorously monitored via blinded caliper measurements with dual quantitative endpoints

[Downloaded from ibj1.pasteur.ac.ir on 2026-10-16]

[DOI: 10.22034/IBJ.30.4.225]

(TGI and AUC), and moderate control variability (SD ≈10% of mean) was addressed through predefined statistical corrections. Finally, formal in vivo synergy modeling was not applied; therefore, the superior efficacy of the combination is described as an enhanced/additive interaction pending mathematical validation.

Collectively, our findings support the development of multi-targeted strategies that integrate standard chemotherapy with tropolone derivatives to overcome therapeutic resistance in GBM. The pronounced antitumor effect of JO-122(2) combined with TMZ underscores its potential as a novel adjunctive therapy for aggressive brain tumors.

5. CONCLUSION

The present study demonstrates that the synthetic tropolone derivative JO-122(2) exhibits significant antitumor activity against U87 MG GBM xenografts. Combining it with TMZ results in greater TGI than using either agent alone. Mechanistically, the enhanced efficacy is associated with coordinated modulation of the p53/MDM2/Bcl-2 axis, characterized by increased levels of p53 and Bax proteins, concomitant downregulation of MDM2 and Bcl-2, and elevated levels of caspase-9. These molecular alterations suggest the engagement of mitochondrial apoptotic signaling, although direct functional validation of caspase cleavage and p53 transcriptional activity remains to be established. While the subcutaneous model does not recapitulate the orthotopic brain microenvironment or blood-brain barrier constraints, the observed efficacy and favorable preliminary safety profile of JO-122(2) warrant further pharmacokinetic and orthotopic evaluations as a potential adjunct to standard GBM treatment.

DECLARATION

Acknowledgments

Not applicable.

Generative AI and AI-assisted technologies

No artificial intelligence was used in the preparation of this manuscript.

Ethical approval

The study was reviewed and approved by the local Bioethics Committee of National Medical Research Centre for Oncology of the Ministry of Health of the Russian Federation (protocol No. 3/221, 2022). All experiments on animals were conducted in compliance with the European Convention for the Protection of Vertebrate Animals (Strasbourg, 1986) and Russian National Standard GOST 33215-2014.

Consent to participate

Not applicable.

Consent for publication

All authors reviewed the results and approved the final version of the manuscript.

Authors' contributions

OIK: supervision and writing–review and editing; AYM: investigation and writing–review and editing; IVG: investigation and writing original draft; NSK: investigation and writing original draft; IVK: investigation and writing–review and editing; DVK and ABS: investigation; AVG: methodology and investigation; AAS: methodology and investigation; SVG and ESB: formal analysis; EER: supervision and writing–review and editing; YAS: investigation and writing original draft; EAG: investigation and writing–review and editing.

Data availability

All relevant data can be found within the manuscript.

Competing interests

The authors declare that they have no competing interests.

Funding

The study was carried out with the financial support of the state assignment "Search for natural and synthetic secondary plant metabolites with antitumor and immunocorrective properties in in vitro and in vivo models", registration number 124022100044-2 from 2024.

Supplementary information

The online version does not contain supplementary material.

REFERENCES

1. Kit O. Glioblastoma multiforme: pathogenesis and molecular markers. Vopr Oncol. 2017;63(5):695-702.
2. Morás AM, Henn JG, Reinhardt LS, Lenz G, Moura DJ. Recent developments in drug delivery strategies for targeting DNA damage response in glioblastoma. Life Sci. 2021;287:120128.
3. Kuznetsova NS, Gurova SV, Goncharova AS, Allilueva E, Gusareva MA, Zinkovich M. Modern approaches to glioblastoma therapy. South Russ J Cancer. 2023;4(1):52-64.
4. Dhuguru J, Ghoneim OA. Quinazoline based HDAC dual inhibitors as potential anti-cancer agents. Molecules. 2022;27(7):2294.
5. Balsa LM, Ruiz MC, de la Parra LS, Baran EJ, León IE.

[Downloaded from ibj1.pasteur.ac.ir on 2026-10-16]

[DOI: 10.22034/IBJ.30.4.225]

Anticancer and antimetastatic activity of copper (II)-tropolone complex against human breast cancer cells, breast multicellular spheroids and mammospheres. J Inorg Biochem. 2020;204:110975.
6. Woodson ME, Mottaleb MA, Murelli RP, Tavis JE. In vitro evaluation of tropolone absorption, metabolism, and clearance. Antiviral Res. 2023;220:105762.
7. Magori N, Fujita T, Kumamoto E. Hinokitiol inhibits compound action potentials in the frog sciatic nerve. Eur J Pharmacol. 2018;819:254-60.
8. Haney SL, Feng D, Kollala SS, Chhonker YS, Varney ML, Williams JT, et al. Investigation of the activity of a novel tropolone in osteosarcoma. Drug Dev Res. 2024;85(1):22129.
9. Ahn JH, Woo JH, Rho JR, Choi JH. Anticancer activity of gukulenin a isolated from the marine sponge Phorbas gukhulensis in vitro and in vivo. Mar Drugs. 2019;17(2):126.
10. Palai BB, Patel SA, Sharma NK, Dixit M. One-pot synthesis of cyclic-aminotropiminium carboxylate derivatives with DNA binding and anticancer properties. Commun Chem. 2022;5(1):179.
11. Kamlyk DV, Khodakova DV, Goncharova AS, Golovinov IV, Galina AV, Shulga AA, et al. Antitumor activity of tropolone JO-122(2) in subcutaneous CDX models of cancer. Res Pract Med J. 2025;12(3):53-60.
12. Kamlyk DV, Khodakova DV, Kolesnikov VE, Snezhko AV, Kolesnikov EN, Gurova SV, et al. Evaluation of the antitumor efficacy of 2-(1,1-dimethyl-1H-benzo[E]indolin-2-yl)-5,6,7-trichloro-1,3-tropolone in vivo. Mod Probl Sci Edu. 2025;3:8-8.
13. Jayakumar T, Liu CH, Wu GY, Lee TY, Manubolu M, Hsieh CY, et al. Hinokitiol inhibits migration of A549 lung cancer cells via suppression of MMPs and induction of antioxidant enzymes and apoptosis. Int J Mol Sci. 2018;19(4):939.
14. Lukbanova EA, Dzhenkova EA, Goncharova AS, Maksimov AY, Komarova EF, Minkin VI, et al. Study of biological activity of 2-quinoline-2-yl-derivative 1,3-tropolone in experiment. Res Pract Med J. 2022;9(2):50-64.
15. Minkin VI, Kit OI, Sayapin YuA, Maksimov AYu, Goncharova AS, Gusakov EA, Tupaeva IO, Krasnikova TA, Kuznetsova NS, Filippova SYu, Chembarova TV, inventors; Southern Federal University; National Medical Research Centre for Oncology, assignees. 2-(1,1-Dimethyl-1H-benzo[e]indolin-2-yl)-5,6,7-trichloro-1,3-tropolone exhibiting cytotoxic activity against A431 skin cancer and H1299 lung cancer cell cultures. Russian Federation patent RU 2810581 C1. 2023 Dec 27. Application 2023128949, filed 2023 Nov 8; published in Bulletin No. 36. Available from: https://new.fips.ru/publication-web/publications/document?type=doc&tab=IZPM&id=E5A9D434-46DD-4B45-B5B2-59E60A649783 [Accessed 2026 Aug 19].
16. Minkin VI, Kit OI, Sayapin YuA, Gusakov EA, Maksimov AYu, Goncharova AS, Tupaeva IO, Krasnikova TA, Gnennaya NV, Kuznetsova NS, Filippova SYu, Chembarova TV, inventors; Southern Federal University; National Medical Research Centre for Oncology, assignees. Agent exhibiting cytotoxic activity against U87MG glioma cell culture. Russian Federation patent RU 2839886 C1. 2025 May 13. Application 2024119879, filed 2024 Jul 15; published in Bulletin No. 14. Available from: https://new.fips.ru/publication-web/publications/document?type=doc&tab=IZPM&id=30040E60-CB8C-4FE6-8023-19C9162835C9 [Accessed 2026 Aug 19].
17. Sayapin YA, Gusakov EA, Tupaeva IO, Dubonosov AD, Dorogan IV, Tkachev VV, et al. Synthesis, structure, ionochromic and cytotoxic properties of new 2-(indolin-2-yl)-1,3-tropolones. Beilstein J Org Chem. 2025;21:358-68.
18. Workman P, Aboagye EO, Balkwill F, Balmain A, Bruder G, Chaplin DJ, et al. Guidelines for the welfare and use of animals in cancer research. Br J Cancer. 2010;102(11):1555-77.
19. Khodakova DV, Kuznetsova NS, Filippova S, Goncharova AS, Galina AV, Gurova SV, et al. The assessment of the cytotoxic activity of 2-(1,1-dimethyl-1H-benzo[e]indolin-2-yl)-5,6,7-trichloro-1,3-tropolone against the human glioblastoma U87 MG cell line. South Russ J Cancer. 2025;6(2):6-13.
20. Kuznetsova NS, Rostorguev EE, Maksimov AY, Vladimirova LY, Hatyushin VE, Golovinov I, et al. Evaluation of the antitumor effect of 2-(1,1-dimethyl-1H-benzo[e]indol-2-yl)-5,6,7-trichloro-1,3-tropolone in in vivo models in monotherapy mode. J Clin Oncol. 2026;44(16):14058.
21. Yang FC, Wang C, Zhu J, Gai QJ, Mao M, He J, et al. Inhibitory effects of temozolomide on glioma cells is sensitized by RSL3-induced ferroptosis but negatively correlated with expression of ferritin heavy chain 1 and ferritin light chain. Lab Invest. 2022;102(7):741-52.
22. Khodakova DV, Vlasov SN, Filippova S, Goncharova AS, Shulga AA, Golovinov IV, et al. Study of the cytotoxic effect of 2-(1,1-dimethyl-1H-benzo[e]indolin-2-yl)-5,6,7-trichloro-1,3-tropolone on the tumor culture of human gastric adenocarcinoma. Mod Probl Sci Educ. 2024;3:24.
23. Gnennaya NV, Chembarova TV, Filippova SY, Mezhevova IV, Novikova IA, Kit OI, et al. Study of the cytostatic effect of a tropolone derivative on primary glioma cell cultures. Vopr Oncol. 2024;70(3):240-1.
24. Mezhevova IV, Filippova SY, Chembarova TV, Gnennaya NV, Goncharova AS, Sayapin YA, et al. Investigation of the cytostatic properties of the novel organic compound 2-(1,1-dimethyl-1H-benzo[e]indolin-2-yl)-5,6,7-trichloro-1,3-tropolone (JO122) on colorectal cancer culture. Vopr Oncol. 2024;70(3):51-2.
25. Gusakov EA, Topchu IA, Mazitova AM, Dorogan IV, Bulatov ER, Serebriiskii IG, et al. Design, synthesis and biological evaluation of 2-quinolyl-1,3-tropolone derivatives as new anti-cancer agents. RSC Adv. 2021;11(8):4555-71.
26. Seo S-K, Hwang C-S, Choe T-B, Hong S-I, Yi JY, Hwang S-G, et al. Selective inhibition of histone deacetylase 2 induces p53-dependent survivin

[Downloaded from ibj1.pasteur.ac.ir on 2026-10-16]

[DOI: 10.22034/IBJ.30.4.225]

downregulation through MDM2 proteasomal degradation. Oncotarget. 2015;6(28):26528-40.
27. Fullagar JL, Garner AL, Struss AK, Day JA, Martin DP, Yu J, et al. Antagonism of a zinc metalloprotease using a unique metal-chelating scaffold: Tropolones as inhibitors of Pseudomonas aeruginosa elastase LasB. Chem Commun. 2013;49(31):3197-9.
28. Haney SL, Allen C, Varney ML, Dykstra KM, Falcone ER, Colligan SH, et al. Novel tropolones induce the unfolded protein response pathway and apoptosis in multiple myeloma cells. Oncotarget. 2017;8(44):76085-98.
29. Wade M, Li YC, Wahl GM. MDM2, MDMX and p53 in oncogenesis and cancer therapy. Nat Rev Cancer. 2013;13(2):83-96.
30. Wang H, Guo M, Wei H, Chen Y. Targeting p53 pathways: Mechanisms, structures and advances in therapy. Signal Transduct Target Ther. 2023;8(1):92.
31. Chen Q, Wang W, Chen S, Chen X, Lin Y. miR-29a sensitizes the response of glioma cells to temozolomide by modulating the P53/MDM2 feedback loop. Cell Mol Biol Lett. 2021;26(1):21.
32. Wang N, Zhu P, Huang R, Sun L, Dong D, Gao Y. Suppressing TRAP1 sensitizes glioblastoma multiforme cells to temozolomide. Exp Ther Med. 2021;22(5):1246.
33. Borrero LJ, El-Deiry WS. Tumor suppressor p53: Biology, signaling pathways, and therapeutic targeting. Biochim Biophys Acta Rev Cancer. 2021;1876(1):188556.
34. Sadeghi Z, Malekzadeh M, Sharifi M, Hashemibeni B. The role of miR-16 and miR-34a family in the regulation of cancers: A review. Heliyon. 2025;11(4):42733.
35. Marei HE, Althani A, Afifi N, Hasan A, Caceci T, Pozzoli G, et al. p53 signaling in cancer progression and therapy. Cancer Cell Int. 2021;21(1):703.
36. Foumani EA, Irani S, Shokoohinia Y, Mostafaie A. Colchicine of colchicum autumnale, a traditional anti-inflammatory medicine, induces apoptosis by activation of apoptotic genes and proteins expression in human breast (MCF-7) and mouse breast (4T1) cell lines. Cell J. 2022;24(11):647-56.
37. Byeon SE, Lee YG, Kim JC, Han JG, Lee HY, Cho JY. Hinokitiol, a natural tropolone derivative, inhibits TNF-α production in LPS-activated macrophages via suppression of NF-κB. Planta medica. 2008;74(08):828-33.
38. Jayab NA, Abed A, Talaat IM, Hamoudi R. The molecular mechanism of NF-κB dysregulation across different subtypes of renal cell carcinoma. J Adv Res. 2025;72:501-14.
39. Komarova EF, Allilueva E, Dzhenkova EA, Goncharova AS, Zaikina EV, Gurova SV, et al. Immunohistochemical assessment of possible anticancer effect mechanisms of 2-(6,8-dimethyl-5-nitro-4chloroquinoline-2-yl)-5,6,7-trichloro-1,3-tropolone in PDX models of lung cancer. South Russ J Cancer. 2023;4(1):6-13.
40. Lee YS, Choi KM, Kim W, Jeon YS, Lee YM, Hong JT, et al. Hinokitiol inhibits cell growth through induction of S-phase arrest and apoptosis in human colon cancer cells and suppresses tumor growth in a mouse xenograft experiment. J Nat Prod. 2013;76(12):2195-202.

[Downloaded from ibj1.pasteur.ac.ir on 2026-10-16]

[DOI: 10.22034/IBJ.30.4.225]